

PHILOSOPHICAL TRANSACTIONS A

rsta.royalsocietypublishing.org

Research



Article submitted to journal

Subject Areas:

Solar System, Planetary Interiors,
Planetary Atmospheres, Planet
Formation

Keywords:

Neptune, interior, atmosphere,
composition

Author for correspondence:

N. A. Teanby

e-mail: n.teanby@bristol.ac.uk

Neptune and Uranus: ice or rock giants?

N. A. Teanby¹, P. G. J. Irwin², J. I. Moses³
and R. Helled⁴

¹School of Earth Sciences, University of Bristol, Wills
Memorial Building, Queens Road, Bristol, BS8 1RJ, UK

²Atmospheric, Oceanic & Planetary Physics, University
of Oxford, Clarendon Laboratory, Parks Road, Oxford,
OX1 3PU. UK.

³Space Science Institute, 4750 Walnut Street, Suite
205, Boulder, CO 80301, USA.

⁴Institute for Computational Science, Center for
Theoretical Astrophysics & Cosmology, University of
Zurich, Winterthurerstr. 190, 8057, Zurich, Switzerland

Existing observations of Uranus and Neptune's fundamental physical properties can be fitted with a wide range of interior models. A key parameter in these models is the bulk rock:ice ratio and models broadly fall into ice-dominated (ice giant) and rock-dominated (rock giant) categories. Here we consider how observations of Neptune's atmospheric temperature and composition (H_2 , He, D/H, CO, CH_4 , H_2O , and CS) can provide further constraints. The tropospheric CO profile in particular is highly diagnostic of interior ice content, but is also controversial, with deep values ranging from zero to 0.5 parts per million. Most existing CO profiles imply extreme O/H enrichments of >250 times solar composition, thus favouring an ice giant. However, such high O/H enrichment is not consistent with D/H observations for a fully mixed and equilibrated Neptune. CO and D/H measurements can be reconciled if there is incomplete interior mixing (ice giant) or if tropospheric CO has a solely external source and only exists in the upper troposphere (rock giant). An interior with more rock than ice is also more compatible with likely outer solar system ice sources. We primarily consider Neptune, but similar arguments apply to Uranus, which has comparable C/H and D/H enrichment, but no observed tropospheric CO. While both ice and rock dominated models are viable, we suggest a rock giant provides a more consistent match to available atmospheric observations.

THE ROYAL SOCIETY
PUBLISHING

© The Author(s) Published by the Royal Society. All rights reserved.

1. Introduction

The internal structure of giant planets is key to understanding how the solar system formed and evolved over the last 4.6 billion years. While multiple spacecraft have visited Jupiter and Saturn - including the Galileo, Juno, and Cassini orbiters - the Voyager 2 flybys of Uranus in 1986 and Neptune in 1989 remain the only spacecraft visits to the icy giants. Information from a single spacecraft flyby combined with subsequent remote observations provide a fairly limited dataset in terms of constraining a planet's internal structure, but some interpretations can be inferred from Uranus and Neptune's fundamental physical properties. Voyager 2 provided the first accurate mass, radius, bulk density, and low-order gravitational harmonics for Uranus and Neptune [1–4]. Early interpretations of planetary bulk densities of 1.3 kg m^{-3} for Uranus and 1.6 kg m^{-3} for Neptune suggested interiors dominated by ices [5,6], although the non-uniqueness of constraints on the interior was considerable, and rock-dominated interiors are also possible [7–10]. The Voyager 2 data have since been reanalysed and augmented with stellar occultations and observations of the orbits of Uranus and Neptune's moons and rings to provide more stringent constraints (reviewed in [9]). While it is clear that Uranus and Neptune have a high fraction of heavy elements, with an overall metallicity mass fraction in the range 0.7–0.9 [9], it is still unclear whether rock or ice is the dominant component. Therefore, Uranus and Neptune's internal structure remains elusive despite decades of observation and modelling. Uranus and Neptune could either be rock giants or ice giants, which has important implications for both their formation and the formation of the solar system as a whole.

Voyager 2 observations of Uranus and Neptune's magnetic fields indicate highly non-dipolar structures [11–14]. Such fields may suggest dynamo action is limited to a conducting near-surface layer [15]. This additionally constrains Uranus and Neptune's interiors by requiring some kind of conducting fluid layer to support dynamo action [16]. In the case of an ice giant this could be a superionic form of water ice that exists at high temperature and pressure [17]. In the case of a rock giant, magma dynamos such as those hypothesised on super-Earths, might be a possibility [18]. However, even though silica is conductive at high pressure, it is most likely to be solid at the high pressures of a planetary core [19]. Mixtures of hydrogen and silicate present in some models [20] might have lower melting points, but it is unknown if they could support dynamo action in Uranus or Neptune's interior because of the wide range of possible conditions and limited high pressure and temperature laboratory data.

Many studies have combined observations of fundamental physical properties and high-pressure thermodynamic equations of state to infer Uranus and Neptune's internal structures [6–8,21–23]. These model-data fits are highly non-unique, but can be split into two main types representing either ice giant or rock giant scenarios [8]. Here we define ice and rock giants as having a rock:ice ratio less than or greater than unity respectively. Ice giant models typically have an outer gas envelope of hydrogen and helium, an intermediate region dominated by ices, and a small core of silicates, iron, and nickel. Such models are up to 90% ice. Rock giant models also have an outer hydrogen/helium gas envelope, but have a bulk interior dominated by silicates mixed with hydrogen/helium along with some ices. These models are up to 70% rock. An ice giant interpretation is currently favoured in the literature. However, an important source of uncertainty is that interiors dominated by rock mixed with light elements such as hydrogen have a similar density to ice mixtures, so could also fit the observed physical properties [5,8]. An additional complication is that, while simple models with distinct layers are appealing, they are not required to fit the observations. Recent work shows there may be significant mixing near internal interfaces, leading to more continuous density profiles [9,20,22]. This widens the range of possible internal structures significantly and leaves open the question of whether silicate-gas mixtures or ice mixtures dominate Uranus and Neptune's interiors [9,24–26].

In summary, there are a wide suite of interior models for Uranus and Neptune, both ice- and rock-dominated, with sharp or gradual layer transitions, but none are definitively preferred by observations of fundamental physical properties. This is severely unconstrained - even by

planetary science standards - and leaves both Uranus and Neptune's origin and the evolution of the outer solar system open to rampant speculation. This uncertainty is one of the major motivations for a new ice giant mission [27–30]. In this review we take an alternative approach by considering if atmospheric observations can provide further insight into internal structure. For Uranus, the atmospheric observations provide less of a constraint than on Neptune as there are currently no detections of tropospheric carbon monoxide on Uranus [31], which is an important part of the ice-giant case. Therefore, we primarily focus on Neptune in this review, but revisit Uranus briefly in the discussion.

2. Atmospheric observations and implications

Here we consider what can be inferred about Neptune's interior from atmospheric remote sensing of the outermost gas envelope layer; either from spacecraft, space-telescopes, or ground-based observatories. Low frequency radio and microwave observations have the ability to probe deepest in the atmosphere. For example, ground based measurements at centimetre wavelengths with the VLA at can probe down to 10's of bars [32,33] and Juno's microwave radiometer observations of Jupiter are sensitive to pressures of up to 1 kbar [34]. These measurements constrain the deep abundances of NH_3 , H_2S , and H_2O , but can contain ambiguities due to limitations on current laboratory spectroscopic data, interference from synchrotron emission, non-uniqueness in the interpretation, and uncertainties in the deep temperature profile [35,36]. Observations at shorter wavelengths have less of these difficulties, but such observations are limited to pressures of less than ~ 10 bar: i.e., the troposphere, stratosphere, and mesosphere. This is well above the major water cloud layer and well mixed region [26,37], so is not ideal for probing the internal structure. Nevertheless, it is what we have available, and with caution some important insights can be gained.

(a) Temperature, thermal emission, and mixing

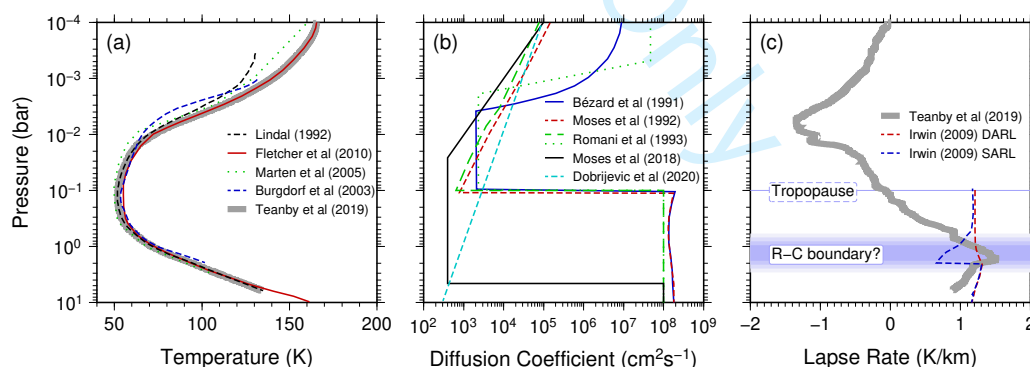


Figure 1. Neptune's atmosphere. (a) Temperature profiles measured by radio occultation and infra-red spectroscopy, illustrating $\sim 5\text{K}$ uncertainty in global mean tropospheric temperature. (b) Eddy mixing profiles constrained by heat flux, composition profiles, and photochemical modelling. All photochemical models require low minimum mixing rates somewhere in the lower stratosphere or upper troposphere ($0.01\text{--}1$ bar), but the location of that minimum is unconstrained. This leads to variations in possible upper troposphere mixing rates of over five orders of magnitude. (c) Observed lapse rate ($-dT/dz$) using a composite $T(p)$ profile, compiled from [38] and [39] by [25], compared to the calculated lapse rate [37]. A low observed lapse rate in the upper troposphere suggests reduced mixing and a radiative convective boundary at ~ 1 bar.

Temperature and vertical mixing are fundamental atmospheric properties and must be considered before attempting to interpret other atmospheric observations. Neptune's nominal temperature profile was determined from Voyager 2's radio occultation, covering pressures from 0.35 mbar to 6.3 bar [38,40]. However, there is a degeneracy between temperature and the mean molecular mass of the atmosphere, which introduces uncertainty into the radio occultation inversion; in particular the assumed methane abundance, the He/H₂ ratio, and the presence of other gases such as nitrogen [40]. Neptune's rotation period is also not well constrained [9], which affects hydrostatic equilibrium calculations used in the radio occultation inversion and introduces further uncertainties [38]. Subsequently, further temperature measurements of the upper troposphere and stratosphere were inferred from infrared spectroscopic observations (for example [39,41,42]), but these suffer from low vertical resolution and also depend on the assumed atmospheric composition. A comparison between different studies reveals an uncertainty in the temperature profile of around 5 K [43,44]. Figure 1a compares various nominal temperature profiles and shows the ~5 K variation. There is also evidence for temperature variations with latitude due to differences in insolation and circulation, particularly at the poles [45].

Total emitted flux measurements show that Neptune emits ~2.6 times the energy it receives from the Sun [46]. This is the highest of any planet in the solar system and requires a significant internal heat source driving vigorous convection up to the observable layers. The high energy emission can be used to estimate the vertical eddy diffusion coefficient K_z from mixing length theory; implying $K_z \sim 10^8 \text{ cm}^2 \text{ s}^{-1}$ in the troposphere [44,47]. However, as the condensable species on Neptune have a higher molar mass than the surrounding atmosphere, it is possible that inhibition of moist convection could occur at pressure levels where condensation is active. For example, in the methane condensation region (~1–2 bar), and also deeper where water condenses (~100–1000 bar) [48–50]. Mixing in the upper atmosphere can be constrained to $\sim 2\text{--}50 \times 10^6 \text{ cm}^2 \text{ s}^{-1}$ from hydrocarbon vertical profiles retrieved from the Voyager ultraviolet occultations [51,52] and from Voyager ultraviolet emission observations of the helium 584 Å line [53]. Between the upper atmosphere and lower stratosphere, mixing can be inferred by comparing observed hydrocarbon profiles to those predicted by photochemical models [52,54–57]. Numerous photochemically produced hydrocarbons have been detected in Neptune's atmosphere, including C₂H₂, C₂H₄, C₂H₆, C₃H₄, C₃H₈, and C₄H₂ [37,57,58], which can be used for this purpose. Photochemical models require a relatively low eddy diffusion coefficient somewhere in the lower stratosphere or upper troposphere to prevent excessive loss of stratospheric hydrocarbons by mixing into the deep interior, but have little sensitivity to what is happening below that minimum. Figure 1b compares eddy diffusion profiles from various studies. Typically a value of $K_z = 10^8 \text{ cm}^2 \text{ s}^{-1}$ is adopted throughout the troposphere [59], with the minimum eddy diffusion coefficient occurring in the lower stratosphere, although this is probably too gross a simplification. The most recent photochemical models arbitrarily extend the mixing minimum into the troposphere [57,60], but model results are generally not sensitive to this lower boundary condition. Therefore, mixing in the upper troposphere is currently not well constrained, either by photochemical model comparisons or the emitted heat flux.

Further insight into mixing can be gained by comparing the measured tropospheric lapse rate to that expected from adiabatic advection [25]. If the measured lapse rate is greater than the adiabatic lapse rate then the atmosphere can be expected to be unstable with significant mixing occurring. In the region of methane condensation (~1–2 bar), it is not currently possible to determine a precise pressure level where the temperature profile becomes super-adiabatic because of uncertainties in Neptune's methane vertical profile [48] and the co-dependence of the derived temperature profile on assumed atmospheric mean molecular mass [38,40]. However, an approximate comparison can still be made. Figure 1c compares the observed lapse rate ($-dT/dz$) from the composite temperature profile in [25], which is a combination of the radio occultation [38] and infra-red [39] temperature profiles, with the calculated dry adiabatic lapse rate (DALR) and saturated adiabatic lapse rate (SALR) for a H₂/He/CH₄ atmosphere [37]. The observed lapse rate is less than both the calculated DALR and SALR for pressures below ~1 bar, indicating

that vigorous mixing is unlikely in the uppermost troposphere (~ 0.1 – 1 bar), no matter the CH_4 saturation state of the atmosphere. This suggests a radiative convective (R-C) boundary, where the majority of thermal emission originates, occurs at ~ 1 bar on Neptune. This is compatible with potentially suppressed moist convection caused by methane condensation [48]. Furthermore, as noted by [25] the brightness temperature of Neptune at $100\ \mu\text{m}$ is $\sim 60\ \text{K}$ [41], suggesting an emission level of 0.5 – 1 bar and placing the R-C boundary at a similar level. These inferences based on lapse rate are also entirely consistent with reduced mixing in the upper troposphere as suggested by the non-detection of disequilibrium species PH_3 in the upper troposphere [25].

(b) Composition

(i) He/H_2

Neptune's observable atmosphere is primarily hydrogen and helium [61,62]. The He/H_2 ratio was found to be 0.15 ± 0.03 by volume for a nominal nitrogen abundance of 0.003 using a combination of Voyager 2 radio occultation and InfraRed Interferometer Spectrometer (IRIS) observations [63]. This is close to the protosolar He/H_2 ratio of 0.17 [64] and may suggest H_2 and He gas were captured directly from the solar nebula. However, [63] show that nitrogen abundances from 0 – 0.006 can also provide reasonable fits to the Voyager IRIS spectra, resulting in possible He/H_2 ratios of 0.08 – 0.22 by volume and leaving open the possibility that Neptune could have sub-solar or super-solar He/H_2 . Nevertheless, the fact that Neptune's atmosphere is primarily composed of hydrogen and helium implies Neptune had to reach sufficient size for direct gravitational accretion fairly rapidly, because the lifetime of the protosolar nebula is estimated at ≤ 10 Myr [26,65]. Therefore, the hydrogen and helium abundance do not discriminate between ice and rock giant interior structures, but are important when considering hydrogen sources for interpretation of the D/H and O/H observations.

(ii) C/H from CH_4

On Neptune methane does not condense until ~ 1 – 2 bar, meaning that the abundance at higher pressures can be considered representative of Neptune's interior, assuming the interior is fully mixed. Neptune's tropospheric methane varies significantly with latitude, but has a globally-averaged volume mixing ratio of ~ 2 – 5% for pressures deeper than the condensation level [66–69]. This large range of abundances shows that, even below the condensation level, condensable species can exhibit considerable variation due to atmospheric dynamics. Dynamics is also thought to cause the large variations in Jupiter's ammonia distribution recently observed at ~ 10 bar by Juno [70,71]. These variations increase the uncertainty on Neptune's deep CH_4 abundance and raise doubts about how representative the measured CH_4 abundance really is of interior composition. Nevertheless, CH_4 is the major carrier of carbon in Neptune's atmosphere and, if its abundance is representative of the interior, implies a C/H enrichment of 50 – 100 times solar [64]. To date this remains the most reliable and direct indicator of elemental enrichment in Neptune [26], despite the large uncertainties.

(iii) D/H from H_2

The D/H ratio is also an important indicator of interior composition and formation [26, 72]. Enrichment in Neptune's D/H ratio compared to solar composition is thought to be due to a significant fraction of enriched protoplanetary ices being mixed into Neptune's interior fluid envelope. D/H in Neptune's atmosphere is $4.1 \pm 0.4 \times 10^{-5}$, derived from Herschel observations of hydrogen [24]. This is around twice as enriched as the protosolar ratio of $(\text{D}/\text{H})_{\text{proto}} = 2.25 \pm 0.35 \times 10^{-5}$ inferred from observations of Jupiter by ISO and Cassini [73,74]. Present day ice reservoirs, including icy moons, comets, and Kuiper belt objects (KBOs), have variable D/H in the range $(\text{D}/\text{H})_{\text{ices}} = 15$ – 60×10^{-5} [26,75–77]. Deriving an interior ice fraction from Neptune's D/H ratio is not straight forward and depends on many assumptions. Consider

a simple case where we assume: 1) present day ices have similar D/H ratios to neptunesimals (planetesimals which formed Neptune); 2) Neptune has a rocky core overlain by an interior fluid envelope and an outer gaseous fluid envelope; 3) the neptunesimals' rock component is sequestered into the planetary core; and 4) the neptunesimals' ice component is well mixed and thermodynamically equilibrated between Neptune's internal fluid and outer gaseous envelopes, such that the measured D/H ratio is representative of the interior. In this case we can estimate the proportion of ices in Neptune's combined fluid envelope following an approach similar to [72]:

$$\left(\frac{D}{H}\right)_{env} = x \left(\frac{D}{H}\right)_{proto} + (1-x) \left(\frac{D}{H}\right)_{ice} \quad (2.1)$$

where, x is the mole fraction of H_2 accreted directly from the protosolar nebula, $(1-x)$ is the mole fraction of H_2 supplied by ices (in the form of water), and $(D/H)_{env}$ is the observed atmospheric value. Under the above assumptions this implies $x=0.85-0.97$, i.e., $<15\%$ ice by mole fraction. This can be used to infer an envelope value for $O/H = (1-x)/(2x + 2(1-x))$, i.e. atoms of O from H_2O / atoms of H from H_2 and H_2O . The overall relation between D/H and O/H in Neptune's fluid envelope under these simple assumptions is then:

$$\left(\frac{O}{H}\right)_{env} = \frac{1}{2} \left[\left(\frac{D}{H}\right)_{env} - \left(\frac{D}{H}\right)_{proto} \right] / \left[\left(\frac{D}{H}\right)_{ice} - \left(\frac{D}{H}\right)_{proto} \right] \quad (2.2)$$

corresponding to $(O/H)_{env}=0.02-0.07$. This implies an O/H enrichment in Neptune of 30–130 times the solar O/H value of 5.4×10^{-4} [64] in the fluid envelope (i.e., not including the core if present). However, if there were incomplete mixing and equilibration in the interior, the deep D/H ratio could be much greater than that in the observable atmosphere. In this case the proportion of ice in the interior fluid envelope could be much larger.

One argument against incomplete mixing and equilibration is that Uranus' D/H ratio of $4.4 \pm 0.4 \times 10^{-5}$ is very similar to Neptune's [24], despite very different internal heat fluxes [46,78] and different internal structures [9,10]. Neptune has a bulk density of 1.6 kg m^{-3} and Uranus is slightly less dense with a bulk density of 1.3 kg m^{-3} [9]. If both planets were formed from similar ices, but in different amounts as indicated by their different densities, and had different internal mixing/equilibration states, the similarity of their D/H ratios would be quite a strange coincidence.

(iv) O/H from CO, H_2O and CS

Neptune's atmospheric carbon monoxide has implications for both external sources and internal bulk composition. As a result, CO has received much observational attention, and has been determined from sub-mm ground-based and space-based telescope observations by many studies [25,39,42–44,79,80]. In sub-mm spectra, CO emission cores are sensitive to the stratospheric abundance, whereas wide absorption wings are sensitive to tropospheric abundance, allowing some details of the CO vertical profile to be determined. Nominal abundances of ~ 1 ppm (parts per million) CO in the stratosphere and ~ 0.1 ppm in the troposphere are required to fit the observed spectra. However, there is significant variation between the different studies (Figure 2) and a consensus on tropospheric abundance has not yet been achieved.

The least controversial aspect of Neptune's CO profile is that there is a significant amount, $\sim 1-2$ ppm, in the stratosphere at millibar pressures. The fact that the stratospheric abundance is greater than the tropospheric abundance implies that Neptune's stratospheric CO must have an external origin [79]. Neptune's stratospheric H_2O abundance of $\sim 1.5-3.5$ ppb (parts per billion) [81] must also have an external origin as water condenses deep in Neptune's interior at $\sim 100-1000$ bar, depending on the deep temperature profile. However, if both CO and H_2O are from the same external source it is not possible to explain the three orders of magnitude abundance difference with a steady state flux of ices, interplanetary dust, or micrometeorites [82]. The most plausible way to explain the stratospheric CO- H_2O discrepancy is if Neptune experienced a large

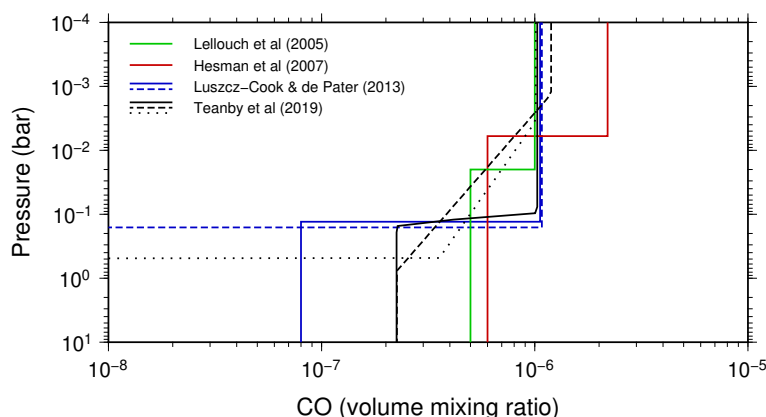


Figure 2. Neptune's CO profile. A comparison of recent studies shows a wide range of CO profiles can fit sub-mm spectra of Neptune. In the stratosphere at ~ 1 mbar there is a broadly consistent 1–2 ppm abundance, but in the troposphere there are inconsistent results ranging from 0–0.5 ppm, indicating the deep CO profile is poorly constrained.

213 kilometre-scale comet impact in the last few hundred to a thousand years and that most of the
 214 cometary H_2O was converted to CO by shock chemistry [79,82,83]. This is supported by recent
 215 observations of CS in Neptune's upper stratosphere in trace amounts (20–200 parts per trillion)
 216 [83]. CS is a shock chemistry product and was observed in Jupiter's stratosphere after the impact
 217 of SL9 [84]. The stratospheric CO abundance is thus not relevant to understanding Neptune's
 218 interior, but its presence does complicate the interpretation of atmospheric composition.

219 Neptune's tropospheric CO does have important implications for the internal composition
 220 and O/H enrichment, but is sadly much more controversial. Some interpretations have deep
 221 tropospheric CO as high as 0.5 ppm [44,79,80], whereas others are consistent with no CO in
 222 the deep troposphere [25,44]. The issue is that tropospheric CO is derived from wide CO line-
 223 wing absorption, which only provides moderate constraints on the CO profile and may not
 224 provide information about pressures higher than ~ 1 bar or so. This is because the line-wing
 225 profile caused by tropospheric CO is degenerate with the uncertain tropospheric temperature
 226 profile. Furthermore, many studies have required multiple observations to be stitched together
 227 to give enough frequency range to cover the entire wing region (e.g., [44,79,80]), which can
 228 introduce baseline shifts and cause additional uncertainties. The exact CO pressure sensitivity
 229 also strongly depends on the uncertain temperature profile and assumptions about the form of the
 230 CO profile itself, making the problem highly non-unique [25]. Given the under-constrained nature
 231 of the problem, simple step-type functions are often used to fit the observations with only three
 232 parameters: tropospheric abundance; stratospheric abundance; and transition pressure. These
 233 profiles are surprisingly good at fitting the observations to within error, but are not likely to
 234 be realistic representations of Neptune's CO profile and extreme caution must be used when
 235 interpreting them - especially the deep abundance. However, at least some CO must be present in
 236 the upper troposphere to explain the observed CO line-wing absorptions and there are currently
 237 two hypotheses about the tropospheric CO profile.

The first and most widely adopted hypothesis is that significant CO exists throughout Neptune's troposphere, well mixed by vigorous convection from the deep interior up to the tropopause [44,79,85]. In thermochemical equilibrium, the mixing ratio of CO is controlled by the net reaction [86]:



238 In the cold upper troposphere, the right-hand-side of reaction (2.3) is strongly favoured, and
 239 CO is not expected to be present in anywhere near observable abundances if thermochemical

equilibrium prevails. However, at high temperatures (>1000 K) in the deep troposphere (>1000 bar), the thermochemical equilibrium abundance of CO is many orders of magnitude larger. To explain ~ 0.1 ppm levels of upper tropospheric CO from an interior source, the atmosphere cannot be in thermochemical equilibrium. Instead, models require a large interior O/H enrichment combined with rapid advection of deep-tropospheric gases, allowing the CO mixing ratio to be quenched at a deep-atmosphere abundance and reaction (2.3) to cease being effective because of the reduced reaction rate at lower temperatures [44,85–87]. For this to happen the mixing timescale must be much less than the loss timescale [44]. The required magnitude of O/H enrichment relative to solar composition depends on details of the chemical scheme, but ranges from 250–650 [44,85,86,88], with an O/H enrichment of ~ 250 being inferred in the most recent study [88].

The second and more fringe hypothesis is that CO only exists in the upper troposphere, at pressures of a few bar or less [25]. In this case tropospheric CO is sourced from the same external comet as the stratospheric CO, not from the deep interior. This allows fitting of the sub-mm spectra without the need for extreme interior O/H enrichment. However, for this to be viable there cannot be vigorous mixing right up to the tropopause, or the upper tropospheric CO would be lost by mixing into the deep interior.

To illustrate the non-uniqueness of spectroscopic sensitivity to tropospheric CO we performed a synthetic retrieval test. We define an atmospheric model based on [25] with a CO profile that has no CO at pressures greater than 1 bar (Figure 3a), representative of an external source only profile [25]. The 1 bar pressure cut-off was chosen to be consistent with the approximate location of the radiative-convective boundary; it is plausible that the abundance of externally sourced CO could be relatively stable at lower pressures than this, but at higher pressures external CO would be lost to the deep interior via vigorous tropospheric mixing. A synthetic spectrum was then generated using the NEMESIS retrieval code [90] for the 115 GHz CO (1-0) line, which is the lowest frequency rotational CO line that probes the deepest in Neptune’s atmosphere (Figure 3b). Random Gaussian noise was applied to this spectrum with a standard deviation of $1/1000^{\text{th}}$ the continuum level (i.e., signal-to-noise = 1000), which is the dynamic range limit of ALMA, the highest sensitivity sub-mm observatory currently available. This observation then represents a best-case scenario for determining the deep CO profile. The CO profile was then inverted from the synthetic spectrum using three types of parameterised profiles: a simple step as commonly used in the literature; a step with a gradient instead of a sharp transition; and an external profile with an upper tropospheric gradient and zero deep abundance. Both gradient profiles could adequately fit the synthetic spectrum within errors, but the simple step slightly under-fits the line wings. However, if small perturbations to the temperature profiles within the 5 K uncertainty were allowed (Figure 3c) then the simple step could fully fit the synthetic spectrum to within errors (Figure 3d). Furthermore, if a slightly lower but still impressive signal-to-noise of 500 was obtained, the step function would be entirely consistent with the measurement without the need for any temperature profile adjustments. The same problem exists the other way around, i.e., an external gradient profile could fit a synthetic made with a step function to within errors. This illustrates the non-uniqueness of obtaining a CO profile on Neptune and explains why there are such a wide range of profiles in the literature. Even with ideal observations, an unrepresentative CO profile can give an excellent fit to the data and provide misleading information about deep CO abundance. The real atmosphere is likely to have some amount of disequilibrium CO being dredged up from the interior, but existing observations are unable to constrain this amount.

3. Interpretation of atmospheric observations

Implications from individual atmospheric observations are often inconsistent and difficult to fit into a single formation model [24,91,92]. Here we consider each of the ice and rock giant interior models and determine what is required to incorporate the atmospheric observations into a self-consistent theory. Figure 4 attempts to illustrate the implications of existing atmospheric

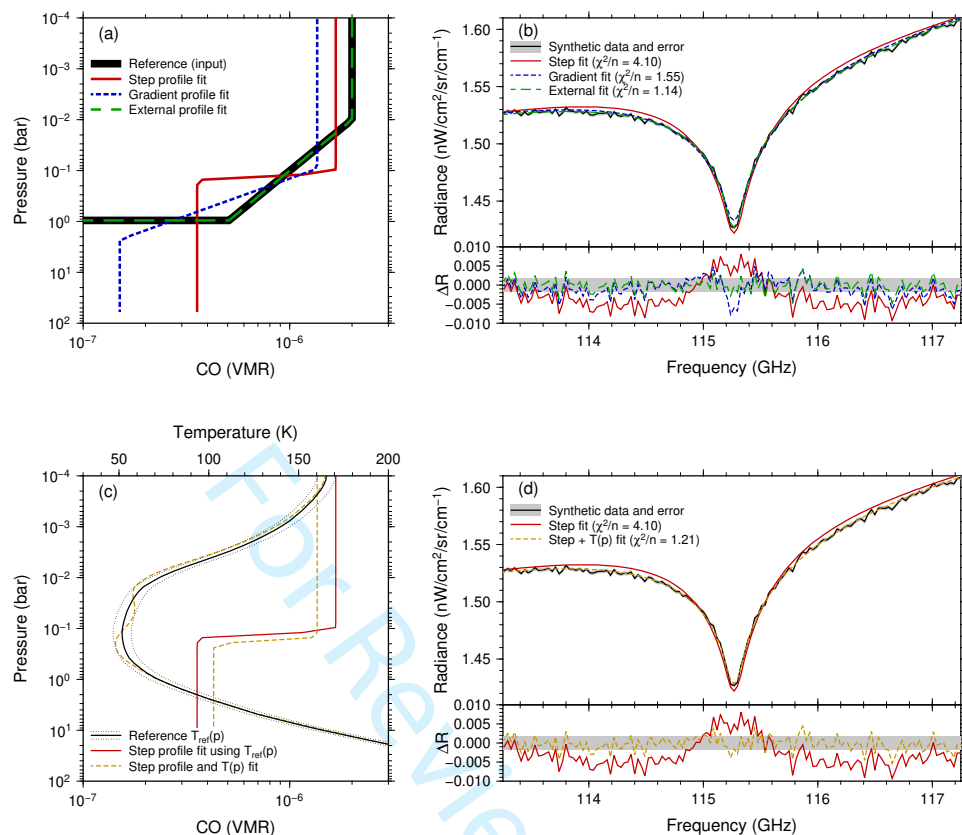


Figure 3. CO (1-0) line sensitivity test. (a) Reference profile used to generate the synthetic spectrum along with best fitting step and gradient profiles. (b) Fits to synthetic data using different profile parameterisations. All profiles provide a reasonable fit to the spectrum, although the step profile under-fits the line wings. (c) A slight adjustment to the temperature profile and step profile transition pressure can drastically improve the fit to the spectrum (d), even though the parameterisation is not representative of the true profile. This illustrates the non-uniqueness of the observations and the challenge of obtaining accurate CO profiles from remote sensing. χ^2/n is the reduced chi-squared misfit and should be around unity for a fit consistent with measurement uncertainties [89]. ΔR is the difference between synthetic data and fitted spectra.

observations for Neptune's interior composition and how they could fit into ice- or rock-dominated interior models. The interdependence of using atmospheric constraints, both on each other and on uncertain assumptions, results in a rather complex and confusing picture. Both rock and ice giants with various degrees of interior mixing can fit the observed fundamental physical properties, which further adds to the uncertainty.

(a) Ice giant

The conventional model of Neptune (and Uranus) is an ice giant, where the interior comprises a large fraction of ices (up to 90% by mass), mostly in the form of water ice. The ice giant model has the advantage of having a large reservoir of interior water, that could act as a conductor for driving the magnetic dynamo. The large fraction of ice is also compatible with extreme O/H enrichment, providing an internal source for tropospheric CO.

However, there are significant problems with having a planet with this much ice. The main issue is that if the interior is fully mixed and equilibrated, the inferred O/H enrichment from

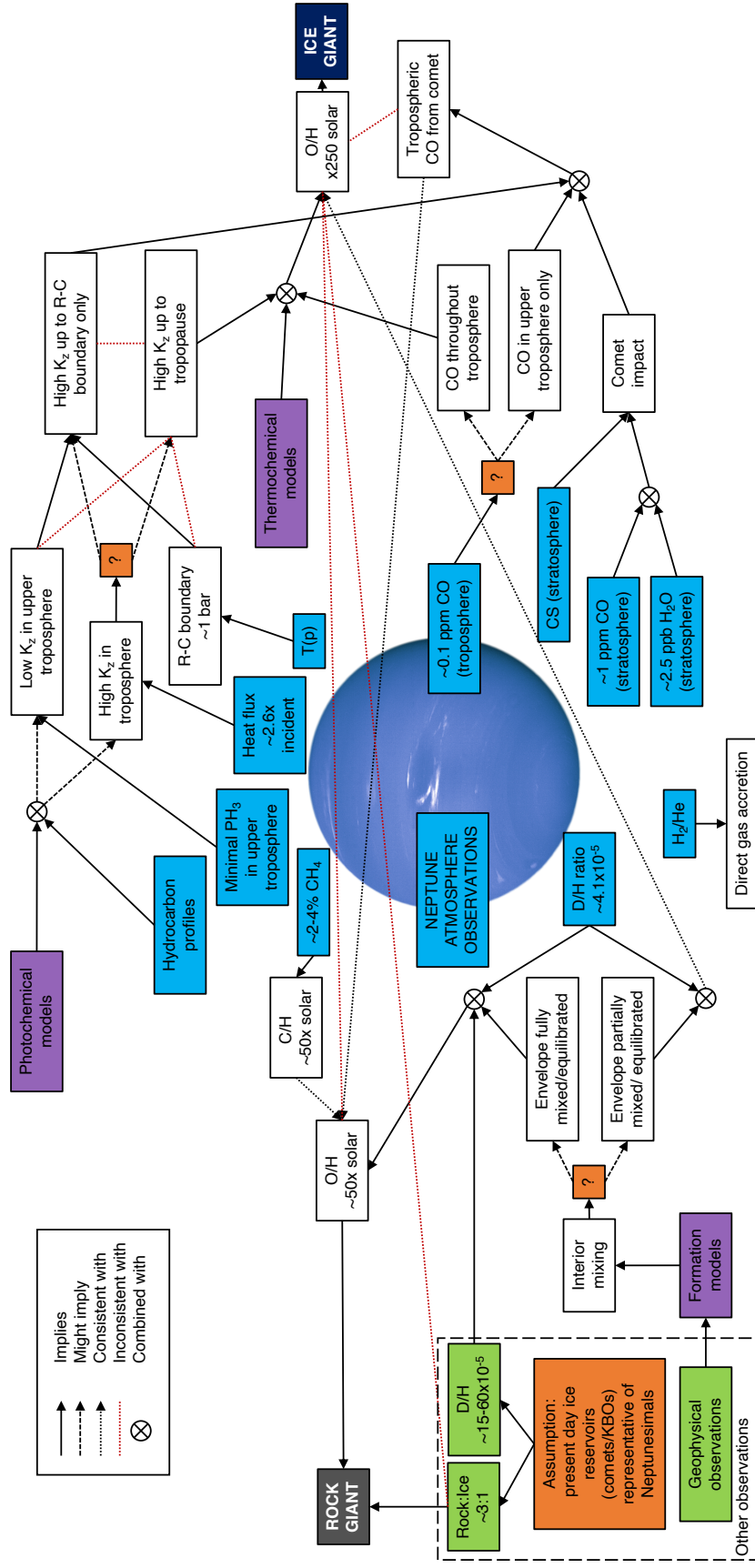


Figure 4. Schematic of Neptune's atmospheric constraints and uncertainties in their interpretation. Key unknowns are shown in orange and imply that it is not possible to definitively distinguish rock and ice giant interiors.

D/H and CO observations are incompatible. O/H enrichment is inferred to be ~ 30 – 130 from the observed D/H ratio, whereas O/H enrichment >250 is inferred based on a deep tropospheric CO mixing ratio of >0.1 ppm. This must be reconciled somehow and there are currently three potential explanations that could be invoked to solve this for the ice giant scenario.

The first solution is if the neptunesimals were depleted in deuterium compared to present day ices and that these exotic ices are no longer present in the solar system, with the justification being that they were all used during planet formation. This seems highly unlikely as it relies on ices that have not been observed anywhere in the solar system and would even be depleted in deuterium compared to Earth's oceans.

A second and more plausible solution is that the interior of Neptune is not completely mixed, so that the measured atmospheric D/H ratio is not representative of the bulk planet. However, the similarity of D/H ratios on Uranus and Neptune [24] is then very difficult to explain if the planets experienced different degrees of mixing, as suggested by their different densities [5,6] and very different heat fluxes [46,78], except by coincidence.

A third alternative is if Neptune formed on the CO ice line. Initial modelling using a static protosolar nebula and a simplified instantaneous condensation scheme suggested that outward diffusion of CO vapour driven by a steep concentration gradient near the ice line, coupled with inward migration of icy pebbles due to gas drag, could result in a high density of CO-rich pebbles at the ice line [93]. If Neptune formed at the ice line then these CO-rich pebbles could explain Neptune's large internal CO source without requiring excessive overall O/H enrichment or H₂O abundance [93]. However, the CO ice line location is very sensitive to rapidly evolving disc conditions [94], with a general tendency to move inwards as the solar nebula cools [95], so considering disc evolution timescales is essential [96]. Recent modelling of condensation rates in the protosolar nebula also shows that production of solids near the ice line is less efficient than previously thought [96], making it difficult to form Neptune at this location effectively. Furthermore, it would be very difficult to form both Neptune and Uranus this way because the ice line would have to migrate from one planet forming location to the other, but remain stable for long enough to build planets in each location, making this scenario even less likely if Neptune and Uranus have similar internal compositions. For Neptune to form on the CO ice line, timescales for planet formation, subsequent planet migration, and ice line evolution must all be compatible, which is difficult to achieve in current models [92,96].

(b) Rock giant

In the rock giant model of Neptune, there are still significant quantities of ice in the interior, but most of the heavy elements are supplied by rock instead of ice. The rock giant model has the advantage that Neptune can be formed from more conventional objects with similar rock-ice ratios to Pluto, giant planet moons, and KBOs. KBOs appear to have a wide range of relative ice compositions from almost pure rock to almost pure ice with smaller objects tending to have lower densities suggesting they are more ice-rich [97]. For example a large object such as Pluto has a relatively high rock:ice ratio of $\sim 3:1$ [98]. Recent observations and modelling show that a rock fraction of ~ 0.7 can in fact fit many of these objects, with variations in porosity explaining the density-size trend rather than variations in ice content [99]. If Neptune were formed from such objects the interior would be rock-dominated and have a much lower O/H enrichment, perhaps around 30–130 times solar. A lower O/H enrichment would also be more consistent with the 50–100 C/H enrichment, assuming typical Neptune formation scenarios, except those in which the heavy elements derive from clathrate hydrates (e.g., [100]). Another advantage of a rock giant is that the reduced fractional content of ice means that the D/H ratio can be explained with primordial ices with a similar D/H enrichment to present day solar system ices, even in the case of complete internal mixing, which allows a greater range of realistic formation scenarios [9]. Additionally, sequestering significant quantities of rocky material in the cores of Uranus and Neptune during planet formation could potentially explain the deficit of refractory material in the surface of the Sun compared to similar stars without planets [101].

354 However, a rock giant interpretation would be at odds with significant tropospheric CO
355 reported by many studies. This could be resolved if CO from a major external source has been
356 slowly transported down from high altitudes to the upper troposphere near the ~ 1 bar region
357 before being removed by faster convective mixing below that level, with the internal source itself
358 remaining much smaller than 0.1 ppm. An accurate CO profile is essential to test this possibility.
359 Another potential problem with a rock giant is how to create the magnetic field, which requires
360 a conductive medium in the interior to support dynamo action. Possibilities include a shallow
361 conductive water-rich layer, sourced from the ice component of the rock-ice neptunesimals, or a
362 conductive silicate-hydrogen mixture of some kind.

363 (c) Summary of interior constraints

364 From the schematic in Figure 4 it is evident that there are four key unknowns, which are essential
365 to fully interpret atmospheric observations in terms of Neptune's interior:

- 366 • The deep extent of CO beyond the upper troposphere, which determines the bulk O/H
367 enrichment.
- 368 • The tropospheric eddy mixing profile, which determines how the CO profile is
369 interpreted.
- 370 • The extent of internal mixing and equilibration within Neptune, which determines how
371 representative atmospheric measurements are of the interior .
- 372 • The source material of neptunesimals, which would allow the D/H ratio to be used to
373 infer bulk ice abundance.

374 The simplest interpretation based on current observations and models is that Neptune is a
375 rock giant, i.e., Neptune formed with more rock than ice (Figure 4). However, under different
376 assumptions both ice and rock giant interpretations are possible.

377 (d) Extension to Uranus

378 While this paper has focused on Neptune, similar arguments could also be made for Uranus. The
379 D/H ratios are very similar on Uranus ($D/H=4.4\pm0.4\times10^{-5}$) and Neptune ($D/H=4.1\pm0.4\times10^{-5}$)
380 [24], suggesting a similar O/H enrichment if Uranus' interior is fully mixed. The tropospheric
381 methane abundance on Uranus is also $\sim 2\text{--}4\%$ [102,103], suggesting a similar C/H enrichment.
382 Many hydrocarbons have also been observed in Uranus' atmosphere [104], but not CS. The
383 main difference in observed atmospheric composition between Uranus and Neptune that has
384 relevance to the interior structure is the measured CO abundance. Uranus' stratospheric CO is
385 $\sim 8\pm 1$ ppb [105], which is much lower abundance than Neptune's ~ 1 ppm. CO has not been
386 detected at all in Uranus' troposphere, with a 3σ upper limit of < 2.1 ppb [31], again much lower
387 than Neptune's ~ 0.1 ppm. Therefore, the case for a rock giant is in fact simpler for Uranus as
388 there is no requirement to dredge up CO from a strongly oxygen enriched interior to explain the
389 tropospheric composition. The lack of tropospheric CO could then be explained by either: lack of
390 a large cometary impact in the rock giant case; or by reduced tropospheric convection in the ice
391 giant case, as inferred from the low emitted infrared flux [78]. The D/H ratio is again the strongest
392 argument in favour of the rock giant scenario, although as for Neptune, for this to have relevance
393 to the interior requires a well mixed fluid envelope [9,24].

394 4. Conclusion

395 Current observational constraints from fundamental physical properties are consistent with both
396 ice and rock giant interpretations of Neptune's internal structure. Further constraints are available
397 from observations of the atmosphere, which we consider in this paper, but it is difficult to
398 definitively interpret these measurements in terms of the planetary bulk composition because

interpretation strongly depends on model assumptions or physical and chemical processes that are not fully understood. In addition, measured abundances are likely influenced by “pollution” from recent comet impact(s), which makes the problem even more challenging. Therefore, observations of Neptune’s atmosphere are somewhat ambiguous and can support either model, depending on what is assumed during the interpretation.

Abundant tropospheric CO has previously been used to argue a preference for the ice giant interpretation, with extreme internal O/H enrichments of >250 , but on closer inspection the evidence for CO at pressures above a few bar is not convincing. Such a model would also most likely require incomplete interior mixing during formation to explain Neptune’s low atmospheric D/H ratio.

Cometary CO and reduced upper tropospheric mixing provides an alternative explanation for Neptune’s CO profile, and is consistent with arguments based on the observed lapse rate and photochemical model comparisons. This could favour a rock giant interpretation, formed from rock-ice mixtures with similar properties to present day solar system objects, resulting in O/H enrichments similar to C/H. This has the advantage of reconciling Neptune’s CO and D/H measurements and using known ice sources.

A similar case can also be made for Uranus being a rock giant. The case for Uranus is in fact more straight forward, as there is no observed tropospheric CO requiring an explanation, either in terms of highly enriched O/H or external cometary source.

Definitively distinguishing between ice and rock giant scenarios on Uranus and Neptune will require a dedicated future mission with orbiter and entry probe elements [28,29,106]. A key measurement to make with such a probe would be the CO profile down to at least 10 bar from a mass spectrometer. However, both CO and N₂ have a molecular mass of 28, making this a difficult observation. N₂ is also predicted to be an important disequilibrium quenched constituent being dredged up from the deep atmosphere, so any instrumentation on an *in situ* Neptune/Uranus probe would need some way of distinguishing CO from N₂ [26,30], which was not possible with the mass spectrometer included on the Galileo probe to Jupiter [107]. If such a CO measurement were possible, it would provide a more definitive measure of Neptune’s O/H enrichment. Such a measurement is not possible from Earth as even the deepest sounding CO 1-0 line can be interpreted in multiple ways and may only be sensitive to a few bar, which is not far enough into the well mixed region to be representative. Measurements of the noble gases are also essential for constraining formation scenarios, but are currently unconstrained as they require in-situ measurement. Neon is soluble in liquid helium so may be depleted, but argon, krypton, and xenon are not so can be used to determine neptunesimal composition, in particular they can distinguish between icy planetestimals, clathrates, and ice line formation scenarios [26].

It would be essential to complement any probe measurements with orbital mapping to provide global context. Observations of Jupiter with Juno show that internally sourced species can be highly variable to high pressures of ~ 10 bar or more [70,71], suggesting the troposphere on Neptune/Uranus may not be well mixed compositionally [106]. Orbital mapping of deep CO at Neptune would be challenging and require a very high specification sub-mm sounder that was carefully designed to be sensitive to deep abundance. Orbital measurements would also vastly improve constraints on fundamental physical properties, particularly high order gravitational coefficients, which can be used to constrain internal structure [9,70,108], and the magnetic field structure and origin.

Uranus and Neptune’s interiors remain a mystery that urgently requires a new mission to solve. This will not only reveal the formation and evolution of these enigmatic worlds, but will also unlock new insights into our solar system’s evolution.

Authors’ Contributions. NAT conceived the study and wrote the initial manuscript. All authors read and contributed to the final manuscript.

Competing Interests. The authors declare that they have no competing interests.

Funding. NAT and PGJI were funded by the UK Science and Technology Facilities Council (STFC). JIM acknowledges support from the NASA Solar System Workings grant 80NSSC19K0536. RH acknowledges support from the Swiss National Science Foundation (SNSF) via grant 200020_188460.

Acknowledgements. The authors are grateful to Mark Hofstadter, Tristan Guillot, and an anonymous reviewer for their insightful comments, which helped improve the manuscript.

References

1. Tyler GL, Sweetnam DN, Anderson JD, Campbell JK, Eshleman VR, Hinson DP, Levy GS, Lindal GF, Marouf EA, Simpson RA. 1986 Voyager 2 radio science observations of the Uranian system: atmosphere, rings, and satellites. *Science* **233**, 79–84.

2. Tyler GL, Sweetnam DN, Anderson JD, Borutski SE, Campbell JK, Eshleman VR, Gresh DL, Gurrola EM, Hinson DP, Kawashima N, Kursinski ER, Levy GS, Lindal GF, Lyons JR, Marouf EA, Rosen PA, Simpson RA, Wood GE. 1989 Voyager radio science observations of Neptune and Triton. *Science* **246**, 1466–1473.

3. Jacobson RA. 2009 The orbits of the Neptunian satellites and the orientation of the pole of Neptune. *Astron. J.* **137**, 4322–4329.

4. Jacobson RA. 2014 The Orbits of the Uranian satellites and rings, the gravity field of the Uranian system, and the orientation of the pole of Uranus. *Astron. J.* **148**, 76.

5. Podolak M, Hubbard W, Stevenson DJ. 1991 Models of Uranus’ interior and magnetic field. In Bergstralh J, Miner E, Shapley Matthews M, editors, *Uranus Space Science Series* pp. 29–61 Tucson. University of Arizona Press.

6. Hubbard WB, Podolak M, Stevenson DJ. 1995 The interior of Neptune. In Cruikshank DP, Matthews MS, Schumann AM, editors, *Neptune and Triton Space Science Series* pp. 109–138 Tucson. University of Arizona Press.

7. Hubbard WB, Nellis WJ, Mitchell AC, Holmes NC, Limaye SS, McCandless PC. 1991 Interior structure of Neptune: comparison with Uranus. *Science* **253**, 648–651.

8. Podolak M, Weizman A, Marley M. 1995 Comparative models of Uranus and Neptune. *Plan. & Space Sci.* **43**, 1517–1522.

9. Helled R, Nettelmann N, Guillot T. 2020 Uranus and Neptune: origin, evolution and internal structure. *Space Sci. Rev.* **216**, 38.

10. Helled R, Fortney J. 2020 The interior structure of Uranus and Neptune: current understanding and open questions. *Phil. Trans. R. Soc. Lond. A* **current issue, under review**.

11. Ness NF, Acuna MH, Behannon KW, Burlaga LF, Connerney JEP, Lepping RP, Neubauer FM. 1986 Magnetic fields at Uranus. *Science* **233**, 85–89.

12. Connerney JEP, Acuna MH, Ness NF. 1987 The magnetic field of Uranus. *J. Geophys. Res.* **92**, 15329–15336.

13. Connerney JEP, Acuna MH, Ness NF. 1991 The magnetic field of Neptune. *J. Geophys. Res.* **96**, 19023–19042.

14. Ness N, Acuña M, Connerney J. 1995 Neptune’s magnetic field and field-geometric properties. In Cruikshank DP, Matthews MS, Schumann AM, editors, *Neptune and Triton Space Science Series* pp. 141–168 Tucson. University of Arizona Press.

15. Stanley S, Bloxham J. 2004 Convective-region geometry as the cause of Uranus’ and Neptune’s unusual magnetic fields. *Nature* **428**, 151–153.

16. Soderlund K. 2020 Ice giant dynamos. *Phil. Trans. R. Soc. Lond. A* **current issue, under review**.

17. Millot M, Hamel S, Rygg JR, Celliers PM, Collins GW, Coppari F, Fratanduono DE, Jeanloz R, Swift DC, Eggert JH. 2018 Experimental evidence for superionic water ice using shock compression. *Nature Physics* **14**, 297–302.

18. Soubiran F, Militzer B. 2018 Electrical conductivity and magnetic dynamos in magma oceans of Super-Earths. *Nature Communications* **9**, 3883.

19. Millot M, Dubrovinskaia N, Černok A, Blaha S, Dubrovinsky L, Braun DG, Celliers PM, Collins GW, Eggert JH, Jeanloz R. 2015 Shock compression of stishovite and melting of silica at planetary interior conditions. *Science* **347**, 418–420.

20. Helled R, Stevenson D. 2017 The fuzziness of giant planets’ cores. *Astrophys. J. Lett.* **840**, L4.

21. Fortney JJ, Nettelmann N. 2010 The interior structure, composition, and evolution of giant planets. *Space Sci. Rev.* **152**, 423–447.

22. Helled R, Anderson JD, Podolak M, Schubert G. 2011 Interior models of Uranus and Neptune. *Astrophys. J.* **726**, 15.

23. Nettelmann N, Helled R, Fortney JJ, Redmer R. 2013 New indication for a dichotomy in the interior structure of Uranus and Neptune from the application of modified shape and rotation data. *Plan. & Space Sci.* **77**, 143–151.

24. Feuchtgruber H, Lellouch E, Orton G, de Graauw T, Vandenbussche B, Swinyard B, Moreno R, Jarchow C, Billebaud F, Cavalié T, Sidher S, Hartogh P. 2013 The D/H ratio in the atmospheres of Uranus and Neptune from Herschel-PACS observations. *Astron. Astrophys.* **551**, 1–9.
25. Teanby NA, Irwin PGJ, Moses JL. 2019 Neptune's carbon monoxide profile and phosphine upper limits from Herschel/SPIRE: implications for interior structure and formation. *Icarus* **319**, 86–98.
26. Atreya SK, Hofstadter MH, In JH, Mousis O, Reh K, Wong MH. 2020 Deep atmosphere composition, structure, origin, and exploration, with particular focus on critical in situ science at the icy giants. *Space Sci. Rev.* **216**, 18.
27. Arridge CS, Agnor CB, André N, Baines KH, Fletcher LN, Gautier D, Hofstadter MD, Jones GH, Lamy L, Langevin Y, Mousis O, Nettelmann N, Russell CT, Stallard T, Tiscareno MS, Tobie G, Bacon A, Chaloner C, Guest M, Kemble S, Peacocke L, Achilleos N, Andert TP, Banfield D, Barabash S, Barthelémy M, Bertucci C, Brandt P, Ceconi B, Chakrabarti S, Cheng AF, Christensen U, Christou A, Coates AJ, Collinson G, Cooper JF, Courtin R, Dougherty MK, Ebert RW, Entradas M, Fazakerley AN, Fortney JJ, Galand M, Gustin J, Hedman M, Helled R, Henri P, Hess S, Holme R, Karatekin Ö, Krupp N, Leisner J, Martin-Torres J, Masters A, Melin H, Miller S, Müller-Wodarg I, Noyelles B, Paranicas C, de Pater I, Pätzold M, Prangé R, Quémerais E, Roussos E, Rymer AM, Sánchez-Lavega A, Saur J, Sayanagi KM, Schenk P, Schubert G, Sergis N, Sohl F, Sittler EC, Teanby NA, Tellmann S, Turtle EP, Vinatier S, Wahlund JE, Zarka P. 2012 Uranus Pathfinder: exploring the origins and evolution of ice giant planets. *Experimental Astronomy* **33**, 753–791.
28. Hofstadter M, Simon A, Atreya S, Banfield D, Fortney JJ, Hayes A, Hedman M, Hospodarsky G, Mandt K, Masters A, Showalter M, Soderlund KM, Turrini D, Turtle E, Reh K, Elliott J, Arora N, Petropoulos A, Ice Giant Mission Study Team. 2019 Uranus and Neptune missions: a study in advance of the next Planetary Science Decadal Survey. *Plan. & Space Sci.* **177**, 104680.
29. Mousis O, Atkinson DH, Ambrosi R, Atreya S, Banfield D, Barabash S, Blanc M, Cavalié T, Coustenis A, Deleuil M, Durry G, Ferri F, Fletcher L, Fouchet T, Guillot T, Hartogh P, Hueso R, Hofstadter M, Lebreton JP, Mandt KE, Rauer H, Rannou P, Renard JB, Sanchez-Lavega A, Sayanagi K, Simon A, Spilker T, Venkatapathy E, Waite JH, Wurz P. 2019 In situ exploration of the giant planets. *arXiv e-prints* p. arXiv:1908.00917.
30. Cavalié T, Venot O, Miguel Y, Fletcher LN, Wurz P, Mousis O, Bounaceur R, Hue V, Leconte J, Dobrijevic M. 2020 The deep composition of Uranus and Neptune from in situ exploration and thermochemical modeling. *Space Sci. Rev.* **216**, 58.
31. Teanby NA, Irwin PGJ. 2013 An external origin for carbon monoxide on Uranus from Herschel/SPIRE?. *Astrophys. J. Lett.* **775**, L49.
32. de Pater I, Massie ST. 1985 Models of the millimeter-centimeter spectra of the giant planets. *Icarus* **62**, 143–171.
33. Hofstadter MD, Butler BJ. 2003 Seasonal change in the deep atmosphere of Uranus. *Icarus* **165**, 168–180.
34. Janssen MA, Oswald JE, Brown ST, Gulkis S, Levin SM, Bolton SJ, Allison MD, Atreya SK, Gautier D, Ingersoll AP, Lunine JJ, Orton GS, Owen TC, Steffes PG, Adumitroaie V, Bellotti A, Jewell LA, Li C, Li L, Misra S, Oyafuso FA, Santos-Costa D, Sarkissian E, Williamson R, Arballo JK, Kitiyakara A, Ulloa-Severino A, Chen JC, Maiwald FW, Sahakian AS, Pingree PJ, Lee KA, Mazer AS, Redick R, Hodges RE, Hughes RC, Bedrosian G, Dawson DE, Hatch WA, Russell DS, Chamberlain NF, Zawadski MS, Khayatian B, Franklin BR, Conley HA, Kempenaar JG, Loo MS, Sunada ET, Vorperion V, Wang CC. 2017 MWR: Microwave Radiometer for the Juno Mission to Jupiter. *Space Sci. Rev.* **213**, 139–185.
35. de Pater I, Mitchell DL. 1993 Radio observations of the planets: the importance of laboratory measurements. *J. Geophys. Res.* **98**, 5471–5490.
36. de Pater I, Richmond M. 1989 Neptune's microwave spectrum from 1 mm to 20 cm. *Icarus* **80**, 1–13.
37. Irwin PGJ. 2009 *Giant planets of our solar system: atmospheres, composition, and structure*. Chichester UK: Springer-Praxis 2nd edition.
38. Lindal GF. 1992 The atmosphere of Neptune - an analysis of radio occultation data acquired with Voyager 2. *Astron. J.* **103**, 967–982.
39. Fletcher LN, Drossart P, Burgdorf M, Orton GS, Encrenaz T. 2010 Neptune's atmospheric composition from AKARI infrared spectroscopy. *Astron. Astrophys.* **514**, A17.
40. Lindal GF, Lyons JR, Sweetnam DN, Eshleman VR, Hinson DP, Tyler GL. 1990 The atmosphere

of Neptune: results of radio occultation measurements with the Voyager 2 spacecraft. *Geophys. Res. Lett.* **17**, 1733–1736.

41. Burgdorf M, Orton GS, Davis GR, Sidher SD, Feuchtgruber H, Griffin MJ, Swinyard BM. 2003 Neptune's far-infrared spectrum from the ISO long-wavelength and short-wavelength spectrometers. *Icarus* **164**, 244–253.

42. Marten A, Matthews HE, Owen T, Moreno R, Hidayat T, Biraud Y. 2005 Improved constraints on Neptune's atmosphere from submillimetre-wavelength observations. *Astron. Astrophys.* **429**, 1097–1105.

43. Lellouch E, Hartogh P, Feuchtgruber H, Vandenbussche B, de Graauw T, Moreno R, Jarchow C, Cavalié T, Orton G, Banaszkiewicz M, Blecka MI, Bockelée-Morvan D, Crovisier J, Encrenaz T, Fulton T, Küppers M, Lara LM, Lis DC, Medvedev AS, Rengel M, Sagawa H, Swinyard B, Szutowicz S, Bensh F, Bergin E, Billebaud F, Biver N, Blake GA, Blommaert JADL, Cernicharo J, Courtin R, Davis GR, Decin L, Encrenaz P, Gonzalez A, Jehin E, Kidger M, Naylor D, Portyankina G, Schieder R, Sidher S, Thomas N, de Val-Borro M, Verdugo E, Waelkens C, Walker H, Aarts H, Comito C, Kawamura JH, Maestrini A, Peacocke T, Teipen R, Tils T, Wildeman K. 2010 First results of Herschel-PACS observations of Neptune. *Astron. Astrophys.* **518**, L152.

44. Luszcz-Cook SH, de Pater I. 2013 Constraining the origins of Neptune's carbon monoxide abundance with CARMA millimeter-wave observations. *Icarus* **222**, 379–400.

45. Fletcher LN, Kaspi Y, Guillot T, Showman AP. 2020 How well do we understand the belt/zone circulation of giant planet atmospheres?. *Space Sci. Rev.* **216**, 30.

46. Pearl JC, Conrath BJ. 1991 The albedo, effective temperature, and energy balance of Neptune, as determined from Voyager data. *J. Geophys. Res.* **96**, 18921–18930.

47. Moses JI, Allen M, Yung YL. 1992 Hydrocarbon nucleation and aerosol formation in Neptune's atmosphere. *Icarus* **99**, 318–346.

48. Guillot T. 1995 Condensation of methane, ammonia, and water and the inhibition of convection in giant planets. *Science* **269**, 1697–1699.

49. Leconte J, Selsis F, Hersant F, Guillot T. 2017 Condensation-inhibited convection in hydrogen-rich atmospheres. Stability against double-diffusive processes and thermal profiles for Jupiter, Saturn, Uranus, and Neptune. *Astron. Astrophys.* **598**, A98.

50. Friedson AJ, Gonzales EJ. 2017 Inhibition of ordinary and diffusive convection in the water condensation zone of the ice giants and implications for their thermal evolution. *Icarus* **297**, 160–178.

51. Yelle RV, Herbert F, Sandel BR, Vervack, Ronald J. J, Wentzel TM. 1993 The distribution hydrocarbons in Neptune's upper atmosphere. *Icarus* **104**, 38–59.

52. Bishop J, Romani PN, Atreya SK. 1998 Voyager 2 ultraviolet spectrometer solar occultations at Neptune: photochemical modeling of the 125–165 nm lightcurves. *Plan. & Space Sci.* **46**, 1–20.

53. Parkinson CD, McConnell JC, Sand el BR, Yelle RV, Broadfoot AL. 1990 He 584 Å dayglow at Neptune. *Geophys. Res. Lett.* **17**, 1709–1712.

54. Bézard B, Romani PN, Conrath BJ, Maguire WC. 1991 Hydrocarbons in Neptune's stratosphere from Voyager infrared observations. *J. Geophys. Res.* **96**, 18961–18975.

55. Bishop J, Atreya SK, Romani PN, Sand el BR, Herbert F. 1992 Voyager 2 ultraviolet spectrometer solar occultations at Neptune: constraints on the abundance of methane in the stratosphere. *J. Geophys. Res.* **97**, 11681–11694.

56. Romani PN, Bishop J, Bézard B, Atreya S. 1993 Methane photochemistry on Neptune: ethane and acetylene mixing ratios and haze production. *Icarus* **106**, 442–463.

57. Moses JI, Fletcher LN, Greathouse TK, Orton GS, Hue V. 2018 Seasonal stratospheric photochemistry on Uranus and Neptune. *Icarus* **307**, 124–145.

58. Moses J, Cavalié T, Fletcher LN, Roman M. 2020 Atmospheric chemistry on Uranus and Neptune. *Phil. Trans. R. Soc. Lond. A* **current issue, under review**.

59. Moses JI. 1992 Meteoroid ablation in Neptune's atmosphere. *Icarus* **99**, 368–383.

60. Dobrijevic M, Loison JC, Hue V, Cavalié T, Hickson KM. 2020 1D photochemical model of the ionosphere and the stratosphere of Neptune. *Icarus* **335**, 113375.

61. Gautier D, Conrath B, Owen T, de Pater I, Atreya S. 1995 The troposphere of Neptune. In Cruikshank DP, Matthews MS, Schumann AM, editors, *Neptune and Triton* Space Science Series pp. 563–628 Tucson. University of Arizona Press.

62. Conrath BJ, Gautier D, Lindal GF, Samuelson RE, Shaffer WA. 1991 The helium abundance of Neptune from Voyager measurements. *J. Geophys. Res.* **96**, 18907–18919.

- 624 63. Conrath BJ, Gautier D, Owen TC, Samuelson RE. 1993 Constraints on N₂ in Neptune's
625 atmosphere from Voyager measurements. *Icarus* **101**, 168–171.
- 626 64. Lodders K. 2010 Solar System abundances of the elements. In Goswami A, Reddy BE, editors,
627 *Principles and Perspectives in Cosmochemistry* pp. 379–417 Berlin, Heidelberg. Springer Berlin
628 Heidelberg.
- 629 65. Podosek FA, Cassen P. 1994 Theoretical, observational and isotopic estimates of the lifetime of
630 the solar nebula. *Meteoritics* **29**, 6–25.
- 631 66. Baines KH, Mickelson ME, Larson LE, Ferguson DW. 1995 The abundances of methane
632 and ortho/para hydrogen on Uranus and Neptune: implications of new laboratory 4-0 H₂
633 quadrupole line parameters. *Icarus* **114**, 328–340.
- 634 67. Karkoschka E, Tomasko MG. 2011 The haze and methane distributions on Neptune from HST-
635 STIS spectroscopy. *Icarus* **211**, 780–797.
- 636 68. Tollefson J, de Pater I, Luszcz-Cook S, DeBoer D. 2019 Neptune's latitudinal variations as
637 viewed with ALMA. *Astron. J.* **157**, 251.
- 638 69. Irwin PGJ, Toledo D, Braude AS, Bacon R, Weilbacher PM, Teanby NA, Fletcher LN, Orton GS.
639 2019 Latitudinal variation in the abundance of methane (CH₄) above the clouds in Neptune's
640 atmosphere from VLT/MUSE narrow field mode observations. *Icarus* **331**, 69–82.
- 641 70. Bolton SJ, Adriani A, Adumitroaie V, Allison M, Anderson J, Atreya S, Bloxham J, Brown S,
642 Connerney JEP, DeJong E, Folkner W, Gautier D, Grassi D, Gulkis S, Guillot T, Hansen C,
643 Hubbard WB, Iess L, Ingersoll A, Janssen M, Jorgensen J, Kaspi Y, Levin SM, Li C, Lunine
644 J, Miguel Y, Mura A, Orton G, Owen T, Ravine M, Smith E, Steffes P, Stone E, Stevenson D,
645 Thorne R, Waite J, Durante D, Ebert RW, Greathouse TK, Hue V, Parisi M, Szalay JR, Wilson
646 R. 2017 Jupiter's interior and deep atmosphere: the initial pole-to-pole passes with the Juno
647 spacecraft. *Science* **356**, 821–825.
- 648 71. Li C, Ingersoll A, Janssen M, Levin S, Bolton S, Adumitroaie V, Allison M, Arballo J, Bellotti
649 A, Brown S, Ewald S, Jewell L, Misra S, Orton G, Oyafuso F, Steffes P, Williamson R. 2017
650 The distribution of ammonia on Jupiter from a preliminary inversion of Juno microwave
651 radiometer data. *Geophys. Res. Lett.* **44**, 5317–5325.
- 652 72. Lecluse C, Robert F, Gautier D, Guiraud M. 1996 Deuterium enrichment in giant planets. *Plan.
653 & Space Sci.* **44**, 1579–1592.
- 654 73. Lellouch E, Bézard B, Fouchet T, Feuchtgruber H, Encrenaz T, de Graauw T. 2001 The
655 deuterium abundance in Jupiter and Saturn from ISO-SWS observations. *Astron. Astrophys.*
656 **370**, 610–622.
- 657 74. Pierel JDR, Nixon CA, Lellouch E, Fletcher LN, Bjoraker GL, Achterberg RK, Bézard B,
658 Hesman BE, Irwin PGJ, Flasar FM. 2017 D/H ratios on Saturn and Jupiter from Cassini CIRS.
659 *Astron. J.* **154**, 178.
- 660 75. Hartogh P, Lis DC, Bockelée-Morvan D, de Val-Borro M, Biver N, Küppers M, Emprechtinger
661 M, Bergin EA, Crovisier J, Rengel M, Moreno R, Szutowicz S, Blake GA. 2011 Ocean-like water
662 in the Jupiter-family comet 103P/Hartley 2. *Nature* **478**, 218–220.
- 663 76. Bockelée-Morvan D, Biver N, Swinyard B, de Val-Borro M, Crovisier J, Hartogh P, Lis DC,
664 Moreno R, Szutowicz S, Lellouch E, Emprechtinger M, Blake GA, Courtin R, Jarchow C,
665 Kidger M, Küppers M, Rengel M, Davis GR, Fulton T, Naylor D, Sidher S, Walker H. 2012
666 Herschel measurements of the D/H and ¹⁶O/¹⁸O ratios in water in the Oort-cloud comet
667 C/2009 P1 (Garradd). *Astron. Astrophys.* **544**, L15.
- 668 77. Altwegg K, Balsiger H, Bar-Nun A, Berthelier JJ, Bieler A, Bochsler P, Briois C, Calmonte U,
669 Combi M, De Keyser J, Eberhardt P, Fiethe B, Fuselier S, Gasc S, Gombosi TI, Hansen KC,
670 Hässig M, Jäckel A, Kopp E, Korth A, LeRoy L, Mall U, Marty B, Mousis O, Neefs E, Owen T,
671 Rème H, Rubin M, Sémon T, Tzou CY, Waite H, Wurz P. 2015 67P/Churyumov-Gerasimenko,
672 a Jupiter family comet with a high D/H ratio. *Science* **347**, 1261952.
- 673 78. Pearl JC, Conrath BJ, Hanel RA, Pirraglia JA, Coustenis A. 1990 The albedo, effective
674 temperature, and energy balance of Uranus, as determined from Voyager IRIS data. *Icarus*
675 **84**, 12–28.
- 676 79. Lellouch E, Moreno R, Paubert G. 2005 A dual origin for Neptune's carbon monoxide?. *Astron.
677 Astrophys.* **430**, L37–L40.
- 678 80. Hesman BE, Davis GR, Matthews HE, Orton GS. 2007 The abundance profile of CO in
679 Neptune's atmosphere. *Icarus* **186**, 342–353.
- 680 81. Feuchtgruber H, Lellouch E, de Graauw T, Bézard B, Encrenaz T, Griffin M. 1997 External
681 supply of oxygen to the atmospheres of the giant planets. *Nature* **389**, 159–162.

- 682 82. Moses JI, Poppe AR. 2017 Dust ablation on the giant planets: consequences for stratospheric
683 photochemistry. *Icarus* **297**, 33–58.
- 684 83. Moreno R, Lellouch E, Cavalié T, Moullet A. 2017 Detection of CS in Neptune's atmosphere
685 from ALMA observations. *Astron. Astrophys.* **608**, L5.
- 686 84. Lellouch E. 1996 Chemistry induced by the impacts: observations. In Noll KS, Weaver HA,
687 Feldman PD, editors, *IAU Colloq. 156: The Collision of Comet Shoemaker-Levy 9 and Jupiter* pp.
688 213–241.
- 689 85. Cavalié T, Venot O, Selsis F, Hersant F, Hartogh P, Leconte J. 2017 Thermochemistry and
690 vertical mixing in the tropospheres of Uranus and Neptune: how convection inhibition can
691 affect the derivation of deep oxygen abundances. *Icarus* **291**, 1–16.
- 692 86. Lodders K, Fegley, Jr. B. 1994 The origin of carbon monoxide in Neptunes's atmosphere. *Icarus*
693 **112**, 368–375.
- 694 87. Prinn RG, Barshay SS. 1977 Carbon monoxide on Jupiter and implications for atmospheric
695 convection. *Science* **198**, 1031–1034.
- 696 88. Venot O, Cavalié T, Bounaceur R, Tremblin P, Brouillard L, Lhoussaine Ben Brahim R. 2020
697 New chemical scheme for giant planet thermochemistry. Update of the methanol chemistry
698 and new reduced chemical scheme. *Astron. Astrophys.* **634**, A78.
- 699 89. Press WH, Flannery BP, Teukolsky SA, Vetterling WT. 1992 *Numerical Recipes*. Cambridge UK:
700 Cambridge Univ. Press 2nd edition.
- 701 90. Irwin P, Teanby N, de Kok R, Fletcher L, Howett C, Tsang C, Wilson C, Calcutt S, Nixon C,
702 Parrish P. 2008 The NEMESIS planetary atmosphere radiative transfer and retrieval tool. *J.*
703 *Quant. Spectro. Rad. Trans.* **109**, 1136–1150.
- 704 91. Ali-Dib M. 2017 A pebbles accretion model with chemistry and implications for the Solar
705 system. *Mon. Not. R. Astron. Soc.* **464**, 4282–4298.
- 706 92. Mousis O, Aguichine A, Atkinson DH, Atreya SK, Cavalié T, Lunine JI, Mand t KE, Ronnet T.
707 2020 Key atmospheric signatures for identifying the source reservoirs of volatiles in Uranus
708 and Neptune. *Space Sci. Rev.* **216**, 77.
- 709 93. Ali-Dib M, Mousis O, Petit JM, Lunine JI. 2014 The measured compositions of Uranus and
710 Neptune from their formation on the CO ice line. *Astrophys. J.* **793**, 1–7.
- 711 94. Panić O, Min M. 2017 Effects of disc mid-plane evolution on CO snowline location. *Mon. Not.*
712 *R. Astron. Soc.* **467**, 1175–1–185.
- 713 95. Dodson-Robinson SE, Willacy K, Bodenheimer P, Turner NJ, Beichman CA. 2009 Ice lines,
714 planetesimal composition and solid surface density in the solar nebula. *Icarus* **200**, 672–693.
- 715 96. Mousis O, Aguichine A, Helled R, Irwin P, Lunine J. 2020 The role of ice lines in the formation
716 of Uranus and Neptune. *Phil. Trans. R. Soc. Lond. A* **current issue, under review**.
- 717 97. Brown ME. 2012 The compositions of Kuiper Belt Objects. *Annual Review of Earth and Planetary*
718 *Sciences* **40**, 467–494.
- 719 98. Simonelli DP, Reynolds RT. 1989 The interiors of Pluto and Charon - structure, composition,
720 and implications. *Geophys. Res. Lett.* **16**, 1209–1212.
- 721 99. Bierson CJ, Nimmo F. 2019 Using the density of Kuiper Belt Objects to constrain their
722 composition and formation history. *Icarus* **326**, 10–17.
- 723 100. Hersant F, Gautier D, Lunine JI. 2004 Enrichment in volatiles in the giant planets of the Solar
724 System. *Plan. & Space Sci.* **52**, 623–641.
- 725 101. Kunitomo M, Guillot T, Ida S, Takeuchi T. 2018 Revisiting the pre-main-sequence evolution of
726 stars. II. Consequences of planet formation on stellar surface composition. *Astron. Astrophys.*
727 **618**, A132.
- 728 102. Karkoschka E, Tomasko M. 2009 The haze and methane distributions on Uranus from HST-
729 STIS spectroscopy. *Icarus* **202**, 287–309.
- 730 103. Sromovsky LA, Fry PM, Kim JH. 2011 Methane on Uranus: the case for a compact CH₄ cloud
731 layer at low latitudes and a severe CH₄ depletion at high-latitudes based on re-analysis of
732 Voyager occultation measurements and STIS spectroscopy. *Icarus* **215**, 292–312.
- 733 104. Orton GS, Moses JI, Fletcher LN, Mainzer AK, Hines D, Hammel HB, Martin-Torres J,
734 Burgdorf M, Merlet C, Line MR. 2014 Mid-infrared spectroscopy of Uranus from the Spitzer
735 infrared spectrometer: 2. Determination of the mean composition of the upper troposphere
736 and stratosphere. *Icarus* **243**, 471–493.
- 737 105. Cavalié T, Moreno R, Lellouch E, Hartogh P, Venot O, Orton GS, Jarchow C, Encrenaz T, Selsis
738 F, Hersant F, Fletcher LN. 2014 The first submillimeter observation of CO in the stratosphere
739 of Uranus. *Astron. Astrophys.* **562**, A33.

- 1
2
3
4
5
6
7
8
9
10
11
12
13
14
15
16
17
18
19
20
21
22
23
24
25
26
27
28
29
30
31
32
33
34
35
36
37
38
39
40
41
42
43
44
45
46
47
48
49
50
51
52
53
54
55
56
57
58
59
60
106. Guillot T. 2019 Uranus and Neptune are key to understand planets with hydrogen
atmospheres. *arXiv e-prints* p. arXiv:1908.02092.
107. Niemann HB, Atreya SK, Carignan GR, Donahue TM, Haberman JA, Harpold DN, Hartle
RE, Hunten DM, Kasprzak WT, Mahaffy PR, Owen TC, Way SH. 1998 The composition of the
Jovian atmosphere as determined by the Galileo probe mass spectrometer. *J. Geophys. Res.* **103**,
22831–22846.
108. Durante D, Parisi M, Serra D, Zannoni M, Notaro V, Racioppa P, Buccino DR, Lari G, Gomez
Casajus L, Iess L, Folkner WM, Tommei G, Tortora P, Bolton SJ. 2020 Jupiter's gravity field
halfway through the Juno mission. *Geophys. Res. Lett.* **47**, e86572.

For Review Only